Reentrant radio-frequency resonator for automated phase-equilibria and dielectric measurements in fluids

Anthony R. H. Goodwin,[a] James B. Mehl,[b] and Michael R. Moldover
National Institute of Standards and Technology, Physical and Chemical Properties Division, Gaithersburg, Maryland 20899

(Received 24 June 1996; accepted for publication 26 August 1996)

A reentrant rf cavity resonator has been developed for automated detection of phase separation of fluid mixtures contained within the cavity. Successful operation was demonstrated by redetermining the phase boundaries of a $CO_2+C_2H_6$ mixture in the vicinity of its critical point. We developed an accurate electrical model for the resonator and used helium to determine the deformation of the resonator under pressure. With the model and pressure compensation, the resonator was capable of very accurate dielectric measurements. We confirmed this by remeasuring the molar dielectric polarizability A_ϵ of argon and obtained the result $A_\epsilon=(4.140\pm0.006)$ cm^3/mol (standard uncertainty) in excellent agreement with published values. We exploited the capability for accurate dielectric measurements to determine the densities of the $CO_2+C_2H_6$ mixture at the phase boundaries and to determine the dipole moment of 1,1,1,2,3,3-hexafluoropropane, a candidate replacement refrigerant. Near the operating frequency of 375 MHz the capacitor in the resonator has an impedance near 14 Ω. This low impedance is more tolerant of electrical conductivity within the test fluid and in parallel paths in the support structures than comparable capacitors operating at audio frequencies. This will be an advantage for operation at high temperatures where some conductivity must be expected in all fluids. Of further value for high-temperature applications, the present rf resonator has only two metal–insulator joints. These joints seal coaxial cables; neither joint is subjected to large mechanical stresses and neither joint is required to maintain precise dimensional tolerances. The resonator is rugged and may be operated with inexpensive electronics.

I. INTRODUCTION

The petroleum recovery and processing industries require extensive measurements to determine the onset of phase separation in mixtures, often at high pressures and high temperatures. This has led to continuing refinement of techniques for automated determination of phase boundaries[1,2] and of phase volumes.[3] An additional motivation for the present research originated in our own laboratory from the need to map the phase boundaries of mixtures of environmentally acceptable working fluids for heat engines and mixtures of such fluids with much less volatile lubricants. Here, we describe a novel, rugged, automated apparatus for determining phase boundaries as a function of temperature and pressure. The apparatus is suitable for operation at elevated temperatures and pressures and with corrosive materials.

The heart of the present apparatus is a reentrant rf cavity resonator that is shown in cross section in Fig. 1. The fluid mixture under study fills the cavity. In use, the cavity is filled to a desired density with a homogeneous mixture. Then the temperature is changed while the pressure and the rf resonance frequency are monitored. When a new phase appears at either the top or the bottom of the cavity, there is a change in the resonance frequency. This change is easily measured and mostly determined by the change in the dielectric constant of the portion of the mixture contained within the annular gap labeled ''capacitor'' in Fig. 1.

When the resonance-frequency data were interpreted using the model developed below (including corrections for pressure-dependent dilation), the reentrant resonator was very well suited for accurately measuring the dielectric polarizability of fluid samples. This additional capability can be exploited in two ways. First, for mixtures such as $CO_2+C_2H_6$ discussed below, the relationship between the polarizability and the density is known. Then the resonance frequency can be used to determine the density of the mixture at the phase boundaries. Second, for other fluids, such as 1,1,1,2,3,3-hexafluoropropane (a candidate replacement working fluid denoted HFC-236ea by the refrigeration industry), the equation of state was measured in our laboratory. However, the polarizability had not been published. In this case, we used data from the reentrant rf resonator to determine the temperature-dependent dipole moment of HFC-236a.

The remainder of this article treats the following topics in order: overview of reentrant cavity resonators and description of test resonators, theory of reentrant resonators, description of experimental methods, measurements of A_ϵ in argon, measurements of the dipole moment of HFC-236a, and finally, measurements of phase equilibria in the mixture $CO_2+C_2H_6$.

II. REENTRANT CAVITY RESONATORS

Reentrant rf cavities have been used to measure accurately the dielectric constant and losses of solid insulators,[4,5]

[a]Presently at: Center for Applied Thermodynamic Studies, University of Idaho, Moscow, ID 83844-0905.
[b]Also at: Physics Department, University of Delaware, Newark, DE 19716-2570.

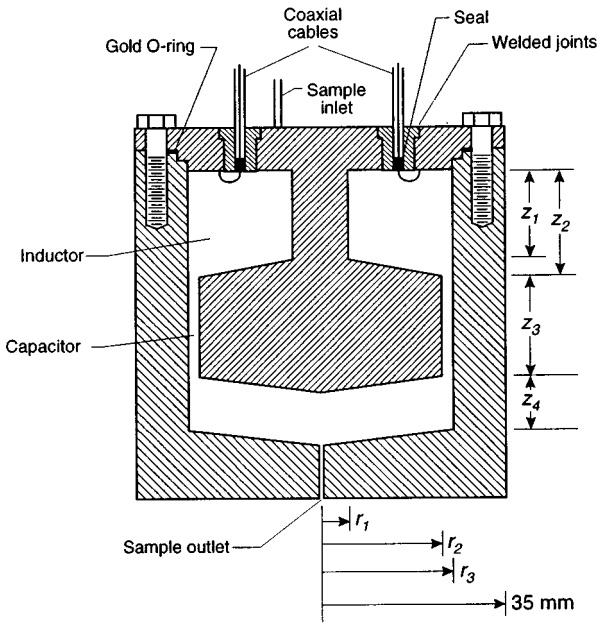

FIG. 1. Reentrant resonator. Approximate dimensions of the brass resonator (in mm) are $r_1=4.96$, $r_2=23.91$, $r_3=25.04$, $z_1=17.0$, $z_2=20.11$, $z_3=19.73$, and $z_4=9.55$.

at frequencies of 50–1000 MHz. They have been used by Van Degrift as pressure sensors,[6] who also proposed that they be used as thermometers, accelerometers, and liquid-level indicators.[7]

The cross section of one of the reentrant resonators that we studied is shown in Fig. 1. Two were manufactured, one was machined from brass and the other from Inconel 625.[8] Apparatus dimensions in this article apply to the brass resonator. However, the two resonators were quite similar.

The body of the resonator was comprised of two metal parts. The lower part was a hollow metal cylinder closed at the bottom. The upper part of the resonator served as a lid to the cylinder and had a cylindrical neck extending down into the cavity. The bottom of the neck expanded into a bulbous, coaxial extension that nearly filled the middle of the cavity. In a first approximation, this reentrant cavity functioned as a parallel *LCR* network with a resonance frequency f_0 given by

$$2\pi f_0 = 1/\sqrt{LC} \tag{1}$$

and a quality factor Q given by

$$Q = 2\pi f_0 L/R. \tag{2}$$

The capacitance, which is mainly determined by the annular gap region labeled capacitor in Fig. 1, equals $C=\epsilon_r C_{\rm vac}$, where $C_{\rm vac}\approx 30$ pF and $\epsilon_r \equiv \epsilon/\epsilon_0$ is the relative electric permittivity of the fluid in the cavity. The inductance $L\approx 5.90$ nH was mostly determined by the toroidal volume labeled ''inductor'' in Fig. 1. Because the relative magnetic permeability $\mu_r \equiv \mu/\mu_0$ of nearly all fluids is negligibly different from 1, the inductance does not change significantly when a fluid fills the cavity. Thus the main dependence of f_0 on sample properties is through a factor $1/\sqrt{\epsilon_r}$. The resonance frequency is approximately 375 MHz when the resonator is evacuated. As an extreme case, it would decrease to approximately 42 MHz if the cavity were filled with liquid water at ambient temperature.

In free oscillations of the cavity at rf frequencies, current flows from one side of the capacitor to the other. The current path from the bulbous extension through the neck, the lid, the gold O-ring, and through the upper portion of the outer cylinder is confined to a thin boundary layer at the surface of metal. The thickness of the layer δ is given by

$$\delta = 1/\sqrt{\pi \mu' \sigma' f} \approx 6.9 \ \ \mu{\rm m}, \tag{3}$$

where σ' and μ' are the electrical conductivity and magnetic permeability of the metal carrying the current. Thus the resistance R, which is inversely proportional to δ, depends upon the operating frequency. When the brass cavity was operated at 375 MHz, $R\approx 12$ mΩ and $Q\approx 920$. Even when constructed from the poorly conducting metal Inconel, $Q\approx 240 \gg 1$. This Q is sufficiently high that the reentrant resonator can easily be used as the frequency-determining element of a rf oscillator. Simple circuits can be used to excite the oscillator,[6,7] and a comparatively inexpensive frequency counter can be used to monitor the changes in the fluid's dielectric constant. (The reentrant cavity does have higher frequency resonances. However, they are very well separated from the 375 MHz mode that we used; the next higher mode is at 2100 MHz.)

The theoretical development below leads to accurate relationships connecting the dielectric constant of the fluid, the geometry of the resonator, the resonance frequency, and Q. The theory accounts for the inductance and resistance correctly to terms of order δ/(cavity dimensions). It accounts for fringing-field contributions [fractional increases of order $2(r_3-r_2)/z_3$] to the capacitance and the unexpected result that corrections to the capacitance on the order of $\delta/(r_3-r_2)$ are not present.

In the present context, the reentrant rf resonator is used to measure the dielectric polarizability of fluids at a frequency near 375 MHz. For this application, we briefly contrast the reentrant rf resonator with two other instruments, namely, the coaxial circular cylindrical capacitors operating at audio frequencies,[9] and leaky microwave cavities[1,2] operating at 8–12 GHz that are used to measure the dielectric polarizability. In these comparisons, we consider only the role of the operating frequency itself and the design constraints resulting from the need for dielectric-to-metal joints.

High-frequency measurements are strongly favored when the test fluid has some conductivity. A conducting dielectric fluid may be characterized by a time constant $\tau=\epsilon/\sigma$. At angular frequencies $\omega=2\pi f$ such that $\omega\tau \gg 1$, the fluid behaves like a lossy dielectric. Capacitance bridges are designed to operate in the regime where the parallel conductivity has a minor influence on the measurement and, in this regime, a fluid-filled resonator may have a Q as large as $\omega\tau$. For pure liquid water at ambient temperature, $\epsilon_r\approx 80$, $\sigma\approx 5\times 10^{-6}/(\Omega\,{\rm m})$, and $\tau\approx 0.14$ ms; thus, the high Q regime is not attained at audio frequencies where capacitance bridges are best operated. As the temperature is raised, the conductivity of most fluids increases and this advantage of high-frequency operation increases. (We note that the dielec-

tric polarizability of polar fluids is strongly frequency dependent at GHz frequencies; thus, quantitative interpretation of GHz data is complicated.)

Even if the test fluid were a perfect insulator, high-frequency measurements are advantageous. A vital design requirement is that the test fluid be able to flow freely through the capacitor. This leads to designs with capacitances no larger than 10–100 pF. At a typical audio frequency of 10 kHz, the electrical impedance of a 30 pF capacitor is 530 kΩ. Thus, operation at audio frequencies requires that the dielectric solids that are used to support the conductors comprising the capacitor have insulation resistances that are large compared with 530 kΩ even when immersed in the sample and when operating at the highest temperatures. These insulators must also have high dimensional stability. Also, the electrical feedthroughs leading from the capacitor to the external instruments must have an insulation resistance that is high compared with 530 kΩ while containing the sample.

In contrast, the 30 pF capacitor in the present reentrant resonator is made entirely of metal; thus, no requirement for dimensionally stable insulators exists. The reentrant resonator's capacitive impedance (14 Ω when operating at 375 MHz) is in series with an inductance whose effective resistance is about 12 mΩ. These relatively low impedances impose only modest requirements on the quality of the feedthrough insulators.

One inspiration for the present work was the application of leaky microwave cavities to the detection of phase transitions by Rogers *et al.*,[1] who coupled a resonant microwave cavity to a sample-filled volume via a sapphire window, and the subsequent use of a similar apparatus by Goodwin *et al.*[10] A portion of the sample adjacent to the window was exposed to the evanescent microwave field. Changes in the dielectric polarizability of that portion of the sample led to changes in the Q of the microwave cavity that were observed. This method operated in the range of 8–12 GHz and can be used with samples that are even more conductive than those that can be used in the reentrant resonator. However, a quantitative model relating the polarizability of the fluid to the geometric and electrical properties of the cavity has not been published; thus, the apparatus was not used for measurements of the polarizability. Also, the construction of the microwave cavity and sample cell, and the electronic equipment used to detect the changes in the microwave Q were much more complex than that required to detect the frequency shifts of a rf reentrant resonator.

III. THEORETICAL MODEL

As noted in Sec. I, the reentrant resonator illustrated in Fig. 1 can be regarded in the lowest approximation as an LC oscillator whose capacitance is associated with the narrow annular gap between the central insert and the outer enclosure. Additional contributions from fringing fields and from the large gap at the bottom of the cavity lead to a total effective capacitance near 30 pF. The capacitor is in parallel with a current path which encloses the annular region near the top of the resonator. The low-frequency inductance of this region can be calculated by noting that the magnetic field generated by an arbitrary superposition of axially symmetric current sheets is purely azimuthal and equal to $I/(2\pi r)$, where I is the sum of all currents encircling the cross section of the toroid. The associated inductance is

$$L_t=\frac{\mu}{2\pi}\left[\frac{z_1r_2-z_2r_1}{r_2-r_1}\ln\left(\frac{r_2}{r_1}\right)+z_2\ln\left(\frac{r_3}{r_2}\right)+z_2-z_1\right]$$
$$\approx 5.90\ \text{nH}. \tag{4}$$

In the brass resonator the currents are confined to a surface layer of thickness δ. Dissipation within this layer can be accounted for by an equivalent series resistance

$$R_t=\frac{\mu'\delta\omega}{4\pi}\left[\frac{z_1}{r_1}+\frac{z_2}{r_3}+\ln\left(\frac{r_3}{r_1}\right)+\sec\theta_t\ln\left(\frac{r_2}{r_1}\right)\right]$$
$$\approx 12.1\ \text{m}\Omega, \tag{5}$$

where $\sec\theta_t$ is the secant of the angle at which the lower surface of the toroid slopes away from the horizontal. For the brass resonator the secant has a numerical value of 1.011, representing a minor correction. The quality factor Q of the resonator, defined as the resonance frequency divided by the full resonance width at $1/\sqrt{2}$ of maximum amplitude, equals $2\pi fL_t/R_t\approx 1160$ for our simple model, in rough agreement with experimental Q's near 920.

The wavelength of electromagnetic radiation at the experimental-frequency is approximately $\lambda\approx 790$ mm. Thus the resonator dimensions, while small fractions of λ, are not sufficiently small that all finite-size effects can be neglected. Both finite-size and dissipative effects can be included in the experimental model by considering the resonator as a pair of coupled coaxial waveguides.

A. Coaxial waveguides

Consider a coaxial waveguide with a dielectric fluid confined to the annular region $a\leqslant r\leqslant b$. Metal of electrical conductivity σ' and magnetic permeability μ' forms the radial boundaries, which are assumed thick compared with the skin depth δ at frequencies of interest. A time dependence proportional to $\exp(i\omega t)$ is assumed.

Stratton[11] presents a full set of equations for coaxial waveguides with walls of finite conductivity. The exact solutions in terms of Bessel functions are unwieldy and unnecessary for most applications. It is more useful to use series approximations of the exact solutions. The important parameters are the series impedance per unit length $\mathscr{Z}=(1+i)\mathscr{R}+i\omega\mathscr{L}$ and the parallel conductance per unit length $\mathscr{Y}=i\omega\mathscr{C}$. Stratton's approximate values for the terms in $\mathscr{Z}$ and $\mathscr{Y}$ are

$$\mathscr{L}=(\mu/2\pi)\ln(b/a), \tag{6}$$

$$\mathscr{R}=\frac{1}{2\pi\sigma'\delta}\left(\frac{1}{a}+\frac{1}{b}\right), \tag{7}$$

$$\mathscr{C}=2\pi\epsilon/\ln(b/a). \tag{8}$$

(These can be modified for a conducting fluid by simply adding the fluid conductivity σ to $i\omega\epsilon$ in the expression for $\mathscr{Y}$.)

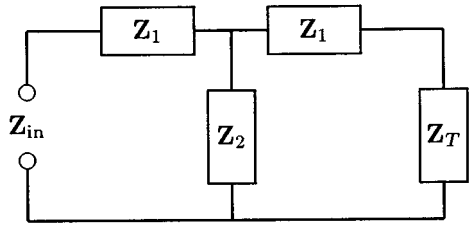

FIG. 2. *T*-equivalent circuit of a waveguide section. The circuit parameters are defined in the text.

The waveguide is further characterized by the propagation parameter $\mathbf{\Gamma} = \sqrt{\mathscr{Y}\mathscr{Z}}$ and the characteristic impedance $\mathbf{Z}_c = \sqrt{\mathscr{Z}/\mathscr{Y}}$. A section of waveguide of length l terminated by an impedance $\mathbf{Z}_T$ can be represented by the *T*-equivalent circuit shown in Fig. 2, where the impedances are

$$\mathbf{Z}_1 = \mathbf{Z}_c \tanh(\mathbf{\Gamma} l/2)$$
$$= (l/2)[i\omega\mathscr{L} + (1+i)\mathscr{R}][1 + \omega^2\mathscr{L}\mathscr{C}l^2/12 + \cdots], \quad (9)$$
$$\mathbf{Z}_2 = \frac{\mathbf{Z}_c}{\sinh(\mathbf{\Gamma} l)} = \frac{1 + \omega^2\mathscr{L}\mathscr{C}l^2/6 + \cdots}{i\omega\mathscr{C}l}. \quad (10)$$

The quantity $\mathscr{L}\mathscr{C} = \mu\epsilon$ is the inverse of the squared propagation speed of the material within the cavity. The quantities $(\omega l)^2\mathscr{L}\mathscr{C}$ are thus small for systems under consideration here. Series terms beyond those displayed can be neglected.

B. Waveguide model of reentrant resonator

The reentrant resonator can be modeled as two sections of coaxial waveguide terminated at the lower end by a cylindrical capacitor. This waveguide model is represented schematically in Fig. 3. The *T*-equivalent parameters $\mathbf{Z}_{t1}$ and $\mathbf{Z}_{t2}$ represent the toroidal section, and the parameters $\mathbf{Z}_{c1}$ and $\mathbf{Z}_{c2}$ represent the capacitive section. The capacitance associated with fringing fields at the upper ends of the capacitive section is C'. The terminal capacitance C_e is the sum of a similar fringing term C'' and the capacitance C_2 of the cylindrical capacitor at the bottom of the resonator. The impedances $\mathbf{Z}'$ and $\mathbf{Z}''$ are associated with radial current flow in the upper and lower surfaces of the inductive section, respectively.

The *T*-equivalent impedances of the inductive section are

$$\mathbf{Z}_{t1} = \tfrac{1}{2}[i\omega L_t + (1+i)R_t'][1 + \omega^2 L_t C_t/12], \quad (11)$$
$$\mathbf{Z}_{t2} = (1 + \omega^2 L_t C_t/6)/(i\omega C_t), \quad (12)$$

with L_t from Eq. (4), $R_t' = \mathscr{R}z_1$, and

$$C_t = 2\pi\epsilon z_1/\ln(r_3/r_1) \approx (0.64 \text{ pF})\epsilon_r. \quad (13)$$

The *T*-equivalent impedances of the coaxial capacitive section are

$$\mathbf{Z}_{c1} \approx i\omega L_c/2, \quad (14)$$
$$\mathbf{Z}_{c2} = (1 + \omega^2 L_c C_1/6)/(i\omega C_1), \quad (15)$$

where

$$C_1 = 2\pi\epsilon z_3/\ln(r_3/r_2) \approx 24 \text{ pF} \quad (16)$$

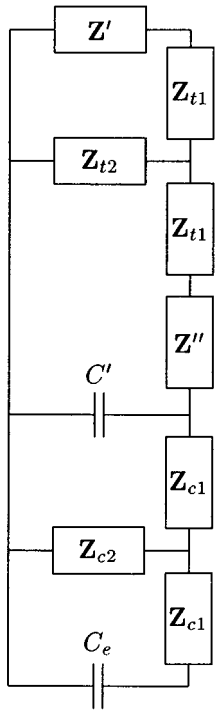

FIG. 3. Schematic representation of reentrant rf resonator. The circuit parameters are defined in the text.

and

$$L_c = (\mu z_3/2\pi)\ln(r_3/r_2) \approx 0.18 \text{ nH}. \quad (17)$$

The finite-size and dissipation terms have been dropped from Eq. (14) because of the smallness of ωL_c. The toroidal section is terminated at its upper end by the impedance $\mathbf{Z}' = (1+i)R'$, where

$$R' = (\mu'\delta\omega/4\pi)\ln(r_3/r_1). \quad (18)$$

The impedance associated with radial current flow at the lower, sloping surface of the toroidal section is given by a similar expression $\mathbf{Z}'' = (1+i)R''$, where R'' is given by Eq. (18) with r_3 replaced by r_2. Shunting susceptances occur at discontinuities in coaxial waveguides.[12] These are represented in Fig. 3 by the capacitances C' and C'', which have been estimated using formulas from Marcuwitz[12] to be $C' \approx (2.3 \text{ pF})\epsilon_r$ at the upper end of the capacitive section, and $C'' \approx (2.6 \text{ pF})\epsilon_r$ at the lower end of the capacitive section. The capacitance of the cylindrical section at the bottom is

$$C_2 \approx \pi\epsilon r_2^2/z_4 \approx (1.7 \text{ pF})\epsilon_r. \quad (19)$$

C. Resonance condition

Conventional circuit analysis can be used to derive a resonance condition for the cavity from the equivalent circuit and the components defined in Sec. III B. It is convenient to represent the resonance frequency as a complex number $\omega = 2\pi(f_0 + ig)$ whose imaginary part corresponds to a damping rate, or equivalently, to the half-width of a resonance line shape. The resonance condition is approximately

$$4\pi^2(f_0+ig)^2$$

$$\approx \frac{1-(1-i)\omega R_t C_4}{L_t(C_4+C_t/3)+L_c[C_e+C_1^2/(3C_4)-C_eC'/C_4]}, \quad (20)$$

where $C_4=C_1+C'+C''+C_2$. At 300 K this predicts a complex resonance frequency f_0+ig of approximately (375 $+i0.16$) MHz, close to experimental values.

IV. RESONANCE FREQUENCY MEASUREMENTS AND ANALYSIS

A network analyzer (HP model 8753B/85047A)[8] was used to measure the transmission characteristics of the resonator. The analyzer excited the resonator through one coaxial feedthrough at a series of fixed frequencies (typically 51–201 frequencies in the work reported here). Both the real and imaginary parts of the signal detected at the other feedthrough were measured by the analyzer and downloaded to the laboratory computer controlling the experiment. A theoretical resonance function

$$\mathbf{w}=\frac{\mathbf{A}f}{f^2-\mathbf{F}^2}+\mathbf{B}, \quad (21)$$

was fit to the complex signal $\mathbf{w}(f)=u(f)+iv(f)$, with the complex constants $\mathbf{F}=f_0+ig$, $\mathbf{A}$, and $\mathbf{B}$ as free parameters. The average rms residual of the fits was typically 0.05% of maximum amplitude. The important parameter used in analysis of experimental results is the resonance frequency f_0, which was typically determined with a fractional standard uncertainty of 3×10^{-7}. The resonance half-width g, an indicator of dissipative processes, was typically determined to a fractional standard uncertainty of 5×10^{-4}.

A typical experimental sequence consisted of a series of resonance frequencies measured as functions of temperature and pressure. The theoretical model for analysis of these data consists of two parts. The first is the real part of Eq. (20), which relates resonance frequency to the relative dielectric constant ϵ_r, the latter an implicit factor in all the capacitance terms in Eq. (20). The second part is the virial expansion of the Clausius–Mossotti equation, which expresses the dependence of ϵ_r on the gas properties:

$$\frac{\epsilon_r-1}{\rho(\epsilon_r+2)}=A_\epsilon+B_\epsilon\rho+\cdots. \quad (22)$$

Here A_ϵ and B_ϵ are the first and second dielectric virials and ρ is the gas density. The latter can be expressed in terms of the pressure p and temperature T by the virial series

$$p=\rho RT[1+B(T)\rho+\cdots], \quad (23)$$

where $B(T)$ is the second density virial coefficient and R is the universal gas constant. A combination of Eqs. (22) and (23) leads to

$$\frac{\epsilon_r-1}{\epsilon_r+2}=A_\epsilon\left(\frac{p}{RT}\right)+(B_\epsilon-BA_\epsilon)\left(\frac{p}{RT}\right)^2+\cdots, \quad (24)$$

which forms the basis for analysis of measurements in nonpolar substances. For polar substances, the temperature dependence of A_ϵ needs to be explicitly included.

The capacitances and inductances in Eq. (20) depend on the resonator dimensions, and hence on temperature and the pressure of the experimental gas. The capacitance C_1, the major component of C_4, is most sensitive to pressure owing to the small annular gap r_3-r_2. As explained below, helium measurements were used to determine the pressure dependence of C_1. The other capacitances and the inductances in Eq. (20) are less sensitive to dimensional changes and were considered to be constant in the analysis of measurements.

Measurements of the resonance half-width g were routinely made in the course of the work. The resulting quality factors $Q=f_0/2g$ were only analyzed for measurements in vacuum, helium, and argon. Essentially equivalent results were obtained for all three cases. The quality factor is weakly dependent upon temperature both through the dependence of the resonance frequency on temperature and through the dependence of the conductivity on temperature. A plot of $1/Q$ vs temperature for the brass resonator had a slope in good agreement with the slope calculated from the resonator model and literature values of the electrical conductivity of brass.[13,14] The experimental values of $1/Q$ exceeded the calculated values by about 30%, however. Earlier measurements with larger coupling loops showed greater excess losses. The excess losses may be due to a combination of remaining overcoupling and surface-roughness effects. Experimental values of $1/Q$ for the Inconel resonator were about a factor of 4 higher than for the brass resonator, and exceeded the calculated values for the Inconel resonator by about 17%. As expected from the weaker dependence of the resistivity of Inconel on temperature, the Q of the Inconel resonator was almost independent of temperature.

V. EXPERIMENTAL PROCEDURES AND MATERIALS

A cross section of one reentrant resonator used in this work is shown in Fig. 1. Both parts of our first reentrant resonator were machined from a single cylindrical billet of yellow brass (65% copper, 35% zinc). The parts met at an interlocking step. The step ensured accurate concentric alignment of the parts when they were bolted together. The cylindrically symmetrical geometry is insensitive to small misalignments and/or to small displacements (either radial or axial) of the two metal parts. The assembled resonator was sealed with a gold O-ring; thus, it served as a pressure vessel. The lower part of the resonator was essentially a hollow cylinder closed at the bottom and with a wall thickness of 10 mm. The upper part of the resonator served as a lid to the cylinder and had a bulbous coaxial extension into the cavity. The assembled resonator had an internal volume of approximately 60 cm^3.

In the brass resonator, the two electrical feedthroughs were formed from stainless-steel, PTFE-insulated, coaxial cables that were sealed into the lid with high pressure conical fittings machined from nylon. For the Inconel resonator, commercially manufactured high-temperature coaxial cables were purchased with sealed ends. These cables were welded into plugs that were themselves welded into the lid of the resonator.

The coupling loops in the prototype resonators were approximately semicircles, 5 mm in diam, oriented in a plane

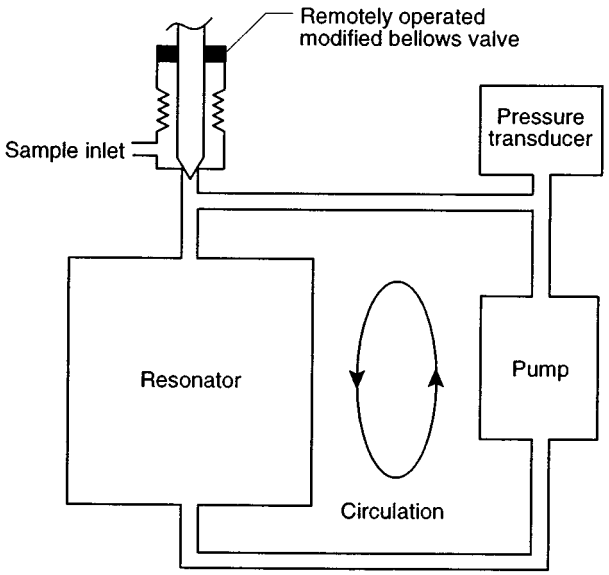

FIG. 4. Schematic diagram of resonator installed in recirculation apparatus. The entire apparatus was immersed in a well-stirred, thermostatted bath.

passing through the axis of symmetry so as to maximize coupling to the magnetic field in the toroidal part of the cavity.

As noted in Sec. IV, a network analyzer was used for high-precision measurements of the resonances frequencies. We also used the resonator as the frequency determining element of a homemade oscillator. A frequency counter was used to monitor the oscillation frequency. We verified that the frequency counter tracked the frequencies determined by the network analyzer to 2×10^{-5} f_0. This much less-expensive instrumentation is satisfactory for determining phase equilibria.

The reentrant resonator, the valve used to seal the test gas within it, and a pressure gauge were immersed in a stirred fluid bath that was thermostatted to within 3 mK. (See Fig. 4.) The temperature was determined with an industrial-grade stainless steel sheathed platinum resistance thermometer calibrated on ITS-90 that was located in a blind hole drilled into the lid of the cell. The thermometer's resistance was measured with a dc digital multimeter operating at a current of 1 mA with a resolution of 0.1 mΩ and a fractional resolution of 5×10^{-5}. When the current was reversed, no differences were observed in the readings of the multimeter. The short-term accuracy of the multimeter was monitored continuously by checking a standard 25 Ω resistor.

For the argon and helium dielectric-constant measurements discussed below, pressures were measured with a fused-quartz Bourdon tube differential pressure gauge. The manufacturer's calibration data indicated that the gauge had a full scale of 10 MPa and was linear to one part in 10^5. We recalibrated it using a piston gauge standard. The zero pressure indication of the gauges varied by up to 1 kPa between checks. The reference port of the gauge was continuously evacuated by a mechanical vacuum pump and monitored with a thermocouple vacuum gauge.

For the refrigerant measurements and for determination of the phase boundary in the mixture ($0.508\ C_2H_6+0.492\ CO_2$), a quartz pressure gauge was used. It had a precision of 0.01 kPa and, after our calibration, appeared to be accurate to 0.1 kPa, a level more than adequate for our purpose. For the other phase boundary determinations with the rf resonator, we used a third pressure measurement system. The fluid was separated from a pressure controller (DH PPC-1)[8] by a differential pressure transducer fitted with a diaphragm which had a nominal range of 550 kPa and was operated as a null instrument. The pressures in the reference line were measured with a second quartz gauge mounted atop the controller. This gauge had a resolution of 0.01 kPa, and, according to the manufacturer, an accuracy of 0.3 kPa.

The gaseous mixtures used were from the same batch used by Weber[15] for equation-of-state measurements. The carbon dioxide and ethane were both research grade materials supplied by Matheson Gas Products, Inc.,[8] with a stated minimum mole fraction purity of 0.999 95 and 0.9996, respectively. We used a diaphragm pump to compress this sample from its low-pressure (700 kPa) storage containers into a 1 ℓ vessel at a pressure greater than 9 MPa. During the compression, the temperature of the gas manifold was maintained at least 20 K above the cricondentherm. After pumping, the mixture was convectively remixed for several weeks.

As shown in Fig. 4, the reentrant resonator was incorporated in a loop with a pump that drew its sample from the bottom of the cavity and pumped it back into the top of the cavity. Such a system was needed to expedite remixing samples once they had separated into phases of differing composition. To facilitate remixing, crevices and ''dead'' volumes were kept to a minimum. We minimized the chances of trapping droplets and bubbles in the resonator by machining conical surfaces on the bulbous extension to the lid and by locating the sample outlet at the center of a conical surface at the very bottom of the resonator.

The design of the circulating pump was adapted from the literature.[16–19] The body of the pump was a 100-mm-long cylinder that had been bored and honed to a 6 mm i.d. Each end of this cylinder was fitted with a restraint that prevented the piston from exiting the cylinder during operation. The top of the vertically mounted piston was fitted with a check valve comprised of a sapphire sphere atop an orifice. The piston was constructed from magnetic, type 440 stainless steel. It has a length of 31 mm and fits smoothly inside the cylinder. In use, the piston was rapidly raised by pulsing an external electromagnet. The upward motion of the piston pumped the sample and forced the sphere on to an orifice in the center of the piston closing the check valve. The ball was raised off this orifice, which opened the valve as the piston fell back to its initial position at the base of the cylinder. When the sphere was in the raised or the free-fall position, fluid could flow through the piston from the lower portion of the cylinder and into the upper part of the cylinder, thereby equalizing the pressure. A typical pumping rate was 0.3 cm^3/s with a pressure head of 100 Pa.

To ensure efficient mixing, the volume of the valve used to admit the sample to the resonator was kept to a minimum and the differential pressure transducer was placed at the

outlet of the pump where it was flushed by the circulating sample.

To obtain phase boundaries of a fluid mixture under precisely controlled conditions, the following operations were used: (1) The resonator and capillary filling lines were baked at 360 K under vacuum; (2) the homogeneous sample was slowly expanded into the cavity; (3) when the required pressure had been attained the resonator was sealed and its contents remixed until the frequency f_0 and pressure p had been stable to within preset limits; (4) the apparatus was cooled to within 5 K of the known phase envelope and the isochore commenced; (5) at each of the 0.25 K temperature steps the frequency, temperature, and pressure were measured; (6) after the phase transition had been determined, the cell was returned to a temperature 20 K above the transition, and the sample was remixed; (7) when the sample was homogeneous, as indicated by measurements of resonant frequency and pressures, a small quantity of fluid was expanded out of the resonator; and (8) steps (4)–(7) were repeated as appropriate.

The phase boundaries were also determined from capacitance measurements with a conventional capacitor and a capacitance bridge (Andeen Hagerling model 2500E)[8] operating at a frequency of 1 kHz with a precision of better than 1×10^{-6} pF. The capacitor used for these additional measurements had been constructed by Younglove and Straty.[9] It has a nominal ambient capacitance of 33 pF. Its top plate was modified so that a resistance thermometer could be placed in contact with the fluid within the cell. Its coaxial, cylindrical electrodes were held in place by cones at each end and insulated with a 12-mm-thick Kapton[8] polymer sheet.

VI. MEASUREMENTS IN PURE GASES

A. Calibration with helium

Helium is an appropriate calibration gas. Its molar polarizability A_ϵ is small and known from the theoretical work of Weinhold[20] to be 0.517 248 cm^3/mol to very high accuracy. The second dielectric virial coefficient B_ϵ is also small. A review by White and Gugan[21] lists experimental values of B_ϵ at room temperature in the range (-0.13 ± 0.02) cm^6/mol^2 and theoretical values spanning a somewhat wider range. Thus B_ϵ is much smaller in magnitude than the product of A_ϵ and the second density virial coefficient (11.5 cm^3/mol at 323.15 K) and hence of marginal importance in the present application.

Resonance frequencies were measured in helium along several isotherms between 273 and 373 K. Typically ten measurements were taken at uniform pressure increments up to a maximum pressure near 300 kPa. These measurements were repeated whenever the apparatus was reassembled following modifications. An initial series of six isotherms at nominal 10 K increments between 280 and 330 K was used to determine the temperature and pressure dependence of the capacitance C_1 in Eq. (20).

The helium data were analyzed as follows. The molar polarizability was held fixed at its theoretical value. Its dielectric constant ϵ_r could thus be calculated from Eq. (24) and the virial equation of state. A factor ϵ_r was included in the calculation of all the capacitances in Eq. (20). A thermal correction factor $(1+\alpha t)$, where $t=(T-273.15\ \mathrm{K})/\mathrm{K}$ and α is the coefficient of linear expansion, was applied to all the inductances and capacitances. The capacitance C_1 is much more sensitive to pressure that the other circuit parameters. It was corrected for pressure through a factor $(1+\beta p)$. The pressure dependence of the other terms was neglected. The sum of the squared differences between the calculated and experimental resonance frequencies was minimized, with $C_{1,0}=C_1|_{t=0}$, α, and β as free parameters. The best fit was obtained with the parameters

$$C_{1,0}=23.5405\ \text{pF},$$

$$\alpha=19.44\times10^{-6}/\mathrm{K},$$

$$\beta=-0.720\times10^{-6}/\mathrm{kPa}.$$

The capacitance $C_{1,0}$ determined in the fit is 1% below the value calculated from nominal apparatus dimensions. Because of the sensitivity of the latter to the small annular gap, this is a satisfactory agreement. The coefficient of thermal expansion determined in the fit agrees within a few percent with published values for brass. No improvement in the fit was obtained by introducing a linear temperature dependence of β.

Separate fits were made to the six helium isotherms. For these fits the coefficient of thermal expansion was held constant at the value 19.44×10^{-6}/K, and separate values of $C_{1,0}$ and β were determined. The means and standard deviations of the parameters determined from the fits are

$$C_{1,0}=(23.5405\pm0.0001)\ \text{pF},$$

$$\beta=(-0.718\pm0.006)\times10^{-6}/\mathrm{kPa}.$$

A second set of helium data was taken following disassembly and reassembly of the apparatus. The parameters determined from a fit to the entire second data set are

$$C_{1,0}=23.4955\ \text{pF},$$

$$\alpha=19.44\times10^{-6}/\mathrm{K},$$

$$\beta=-0.717\times10^{-6}/\mathrm{kPa}.$$

The redetermined thermal expansion and dilation coefficients are thus in excellent agreement with the previous values.

Analysis of data taken with other gases requires a value of the dilation coefficient. The value used in further analysis was

$$\beta=(-0.720\pm0.006)\times10^{-6}/\mathrm{kPa}, \tag{25}$$

where the quantity following the $\pm$ symbol is a standard uncertainty.

B. Argon

The dielectric properties of argon are also well known. A series of measurements in argon on six isotherms at nominal 10 K increments between 280 and 330 K were used as a check on the experimental method. The data were first analyzed by varying parameters A_ϵ, $C_{1,0}$, and α, with the dilation coefficient held constant at the value given in Eq. (25). The best fit was obtained with

$A_\epsilon = 4.140\ \text{cm}^3/\text{mol}$,

$C_{1,0} = 23.5405\ \text{pF}$,

$\alpha = 19.37 \times 10^{-6}/\text{K}$.

The value of the dielectric virial A_ϵ is 0.02% above the value reported by Bose and Cole.[22] The excellent agreement of the parameters $C_{1,0}$ and α determined from the argon and helium data suggested a second argon analysis with these parameters fixed at the values determined with helium. The only free parameter in the second fit, A_ϵ was determined to be 4.137 cm^3/mol, which is 0.06% below the value reported by Bose and Cole.

The uncertainty in A_ϵ was estimated as follows. The contribution from the uncertainty in β was determined by repeating the analysis with β incremented and decremented by one standard uncertainty. These changes altered the value of A_ϵ by ± 0.005 cm^3/mol. A second contribution was determined by fits to the individual argon isotherms. The means and standard deviations of the parameters determined from the isotherm fits are

$A_\epsilon = (4.140 \pm 0.003)\text{cm}^3/\text{mol}$,

$C_{1,0} = (23.5404 \pm 0.0001)\ \text{pF}$.

The standard deviation of these values of A_ϵ was combined with the uncertainty arising from the dilation correction to obtain the combined standard uncertainty in our value for the dielectric virial of argon: $A_\epsilon = (4.140 \pm 0.006)\ \text{cm}^3/\text{mol}$.

C. Polar gases

Polar gases have a significant dipole contribution to A_ϵ. The dipole term is temperature dependent. In the simplest case, the temperature dependence is expressed in the Debye equation

$$A_\epsilon = A_\epsilon^{\text{at}} + A_\epsilon^{\text{el}} + \frac{N_A \mu^2}{9\epsilon_0 k_B T}, \tag{26}$$

where A_ϵ^{at} and A_ϵ^{el} are the atomic and electronic contributions, respectively, N_A is the Avogadro constant, k_B the Boltzmann constant, and μ the dipole moment, which itself may have a temperature dependence.

To illustrate the usefulness of the reentrant resonator for measurements of dipole moments, we report here a series of measurements on HFC-236ea. Resonance frequencies were determined at nine temperatures between 273 and 350 K. The maximum pressure for each isotherm was limited to the lower of 150 kPa or 60% of the liquid–vapor equilibrium pressure. The resulting data set consisted of a set of 83 resonance frequencies as functions of pressure and temperature. The gas densities for each pressure and temperature were calculated using the program REFPROP.[23] The theoretical model for the resonance frequencies based on Eqs. (20), (24), and (26) was then fit to the data by minimizing the sum of the squared differences between the experimental and calculated resonance frequencies. For the first fit, the dipole moment in Eq. (26) was assumed to be a linear function of temperature

$$\mu(T) = \mu_1 + \mu_2 t. \tag{27}$$

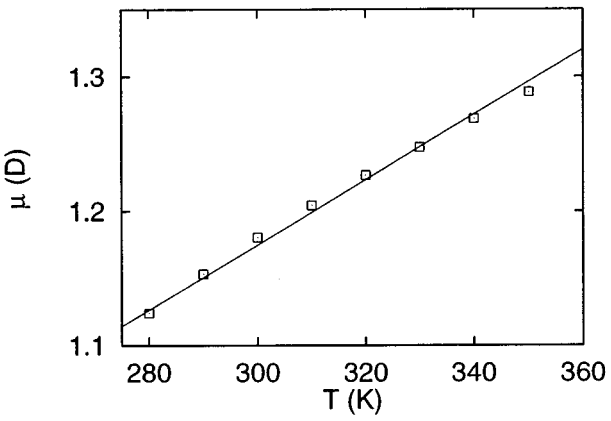

FIG. 5. Dipole moment of 1,1,1,2,3,3-hexafluoropropane (HFC-236ea). The symbols were obtained by separate fits to each isotherm; the straight line was determined by fitting a linear expression for μ to the entire data set.

The additional fit parameters were the capacitance $C_{1,0}$ and the coefficient of thermal expansion α. The parameter A_ϵ was held fixed at values determined from optical measurements as explained below. The dilation coefficient was held constant at the value determined by calibration with helium. The rms frequency residual of the four-parameter fit was 5 kHz, or 0.014% of the average resonance frequency. The parameters representing the dipole moment determined in the fit are $\mu_1 = 1.110$ D and $\mu_2 = 0.0024$ D. The straight line in Fig. 5 corresponds to these parameters.

Each isotherm was also analyzed separately. Only two parameters, the dipole moment and the capacitance $C_{1,0}$ were varied in these fits. The dipole moments determined from these fits, as shown in Fig. 5, have a rms deviation of 0.004 D from the straight line. The rms frequency residuals of the isotherm fits varied from 0.08 to 1 kHz, in contrast with the 5 kHz rms residual for the fit to the entire data set. The relative poorness of the fit to the full data set may be due in part to hysteresis in apparatus dimensions.

As noted above, the electronic and atomic contributions to the polarizability were required for the analysis of polar gases. The electronic contribution A_ϵ^{el} was estimated from measurements of the optical index of refraction of a liquid sample, as described by Goodwin and Morrison,[24] and the atomic contribution A_ϵ^{at} was estimated to be (0.2 ± 0.1) of A_ϵ^{el} using a modification of the rule suggested by Meyer and Morrison.[25] The uncertainty in this estimate is the standard uncertainty estimated from the variance in measured values of the ratio of the atomic to electronic polarizabilities.[25,26] It is the major source of uncertainty in the dipole moments. Reanalysis of the data with $A_\epsilon^{\text{at}} = 0.1 A_\epsilon^{\text{el}}$ increased the dipole moments by an average of 0.03 D. This quantity is the estimated standard uncertainty in the dipole moments. It greatly exceeds the scatter in Fig. 5, as well as the uncertainty due to the uncertainty in β (0.0001 D).

VII. MEASUREMENTS IN MIXTURES

To demonstrate the usefulness of the reentrant resonator for observation of phase boundaries in mixtures, we describe a series of measurements carried out on a sample of the mixture (0.508 C_2H_6 + 0.492 CO_2).

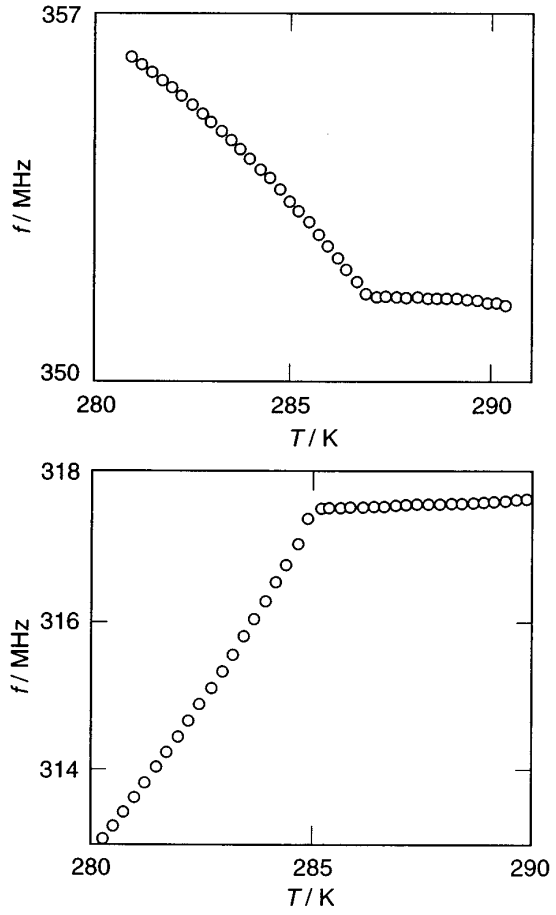

FIG. 6. Frequency of the reentrant resonator filled with the mixture 0.508 $C_2H6+0.492CO_2$. Upper: at the dew point on the isochore $\rho=4.687$ mol/dm^3 where $T_d=(286.98\pm0.06)$ K and $p_d=(5110\pm8)$ kPa. Lower: at the bubble point on the isochore $\rho=12.51$ mol/dm^3 where $T_b=(285.15\pm0.06)$ K and $p_b=(5025\pm15)$ kPa.

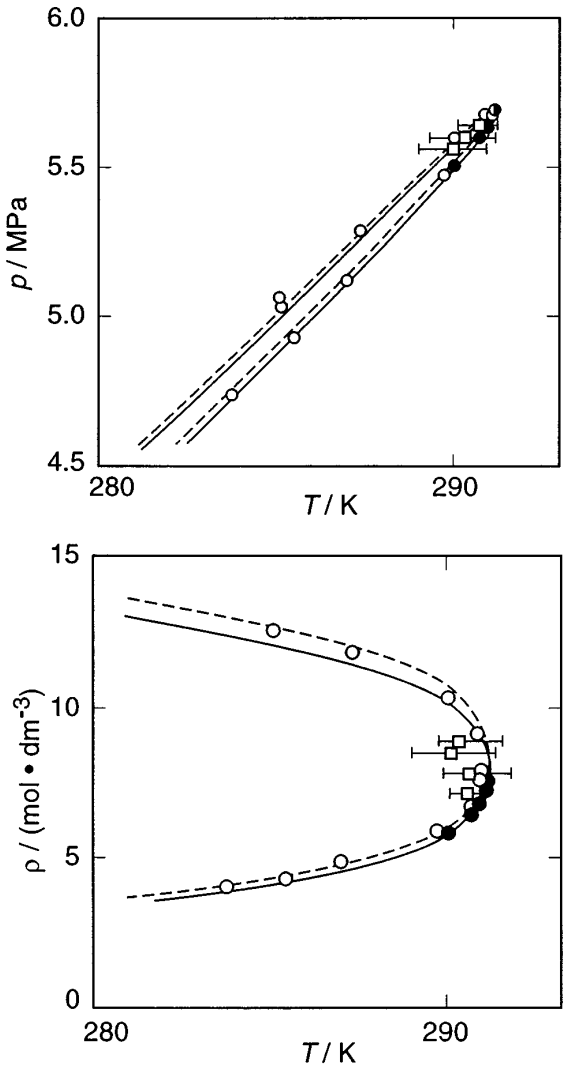

FIG. 7. Upper: pressure vs temperature section; Lower: density vs temperature section; both for the mixture 0.508 $C_2H6+0.492CO_2$. ○, this work, reentrant resonator; ●, this work, concentric cylinder capacitor; □, equation-of-state measurements (Ref. 15); solid line, correlation of literature data (Ref. 27); dashed line, correlation of literature data (Ref. 28).

As the temperature was reduced along an isochore we monitored the resonance frequency, temperature, and pressure. The resonance frequency is shown in Fig. 6 at temperatures close to the dew point along an isochore at a density of 4.687 mol/dm^3. To a good approximation, the density of the sample (and the resonance frequency) did not change until a second phase (either a bubble or a drop) formed. The formation of a second phase near the top or bottom of the reentrant cavity was accompanied by flow of some of the parent phase into or out of the capacitor and by a change in the composition of the first phase.

The results at the top of Fig. 6 are consistent with depletion of gaseous ethane from the capacitor to form liquid elsewhere, presumably near the bottom of the resonator. As the temperature was reduced in steps of 0.25 K, each lasting one hour, the droplet grew and the density of the remainder of the sample, including the sample within the capacitor, decreased. From the results shown in Fig. 6 it was possible to determine the onset of condensation with a resolution limited by the step size to 0.06 K. At the phase transition, $df_0/dT\approx-1$ MHz/K, and the resolution in each frequency measurement was about 0.0001 MHz. Thus the ultimate resolution of phase-boundary detection could be as high as 0.1 mK, if the resolution of the frequency measurement were the limiting factor. As noted earlier, a less-expensive alternative to using the network analyzer for frequency determination is to use the reentrant cavity as the frequency-determining element of an oscillator. The frequency resolution of this approach corresponds to a temperature resolution of order 10 mK.

At precisely the same temperature that df_0/dT had a discontinuity, the temperature derivative of the half-width of the resonance frequency dg/dT also had a discontinuity, as expected because of the frequency dependence of the resonator resistance R_t.

The resonance frequency, shown in the lower part of Fig. 6 near a bubble point at a density of 12.508 mol/dm^3, decreases at the onset of a phase change and the capacitance increases. Presumably the gaseous phase, rich in CO_2, formed near the top the reentrant cavity. At this density $df/dT\approx1.5$ MHz/K. The results provide further evidence for the extraordinary resolution with which phase changes can be detected with this technique.

The phase boundaries of the mixture are shown in a $p(T)$ section in Fig. 7. The figure shows boundaries determined in this work, both with the reentrant resonator and with a conventional concentric-cylinder capacitor operated with a 1 kHz bridge,[9] together with literature values from equation-of-state measurements[15] and from two Leung–Griffiths-type equations of state.[27,28] Considering that these equations of state are based on experimental information independent of ours, the level of agreement is quite remarkable.

The average density of the fluid within the capacitor can be determined from the values of ϵ_r through Eq. (22). In particular, one can estimate the coexisting phase density. This analysis requires a knowledge of $A_\epsilon(x)$, where x is the mole fraction. We assumed, as suggested by Burfield *et al.*,[29] that $A_\epsilon(x)$ was equal to the mole fraction average of the constituents. We determined A_ϵ for each component with the coaxial capacitor[9] and the 1 kHz bridge. The results were $A_\epsilon = 7.34$ cm^3/mol for CO_2 at 1.45 MPa, 293.1 K; and $A_\epsilon = 11.15$ cm^3/mol for C_2H_6 at 2.77 MPa, 293.1 K. Based on the relative-permittivity measurements of vapor–liquid equilibria, and the dielectric-constant measurements for helium and carbon dioxide systems of Burfield *et al.*,[29] we conclude that the uncertainty of our values of density is about 0.5%.

The coexisting phase densities obtained from our analysis are also shown in a $\rho(T)$ projection in Fig. 7 together with values obtained from equation-of-state measurements and smooth curves representing the Leung–Griffiths-type equations of state.[27,28] Again, the agreement is very good and demonstrates the utility of this method as well as the accuracy of the assumption that $A_\epsilon(x)$ for this mixture can be adequately represented by the mole fraction average.

We recall that the resonance frequency depends mainly upon the dielectric constant of the fluid within the capacitor gap; however, there are substantial contributions from the capacitance associated with fringing fields and the capacitance of the space below the bulbous extension of the lid. Thus, when two fluid phases are present in the resonator, the resonance frequency has a complex dependence upon the volume fractions of the phases. Because of this complexity, we have not quantitatively interpreted the data taken when two fluid phases were present in the resonator.

ACKNOWLEDGMENTS

This research was supported in part by the Division of Engineering and Geosciences, Office of Basic Energy Sciences, U.S. Department of Energy, under Contract No. DE-AI05-88ER13823. The authors thank Allan Band of the Electron and Optical Physics Division of NIST for designing and constructing the oscillator circuit.

[1] W. J. Rogers, J. C. Holste, P. T. Eubank, and K. R. Hall, Rev. Sci. Instrum. **56**, 1907 (1985).
[2] F. Fogh and P. Rasmussen, Ind. Eng. Chem. Res. **28**, 371 (1989).
[3] F. Fontalba, D. Richon, and H. Renon, Rev. Sci. Instrum. **55**, 944 (1984).
[4] C. N. Works, T. W. Dakin, and F. W. Boggs, Proc. IRE **33**, 245 (1945).
[5] A. H. Scott, Proc. ISA **11**, 2 (1956).
[6] C. T. Van Degrift, Rev. Sci. Instrum. **45**, 1171 (1974).
[7] C. T. Van Degrift, Proceedings of the 31st Symposium on Frequency Control, Atlantic City, NJ, 1977 (unpublished), p. 375.
[8] In order to describe materials and experimental procedures adequately, it is occasionally necessary to identify commercial products by manufacturer's name or label. In no instance does such identification imply endorsement by the National Institute of Standards and Technology, nor does it imply that the particular product or equipment is necessarily the best available for the purpose.
[9] B. A. Younglove and G. C. Straty, Rev. Sci. Instrum. **41**, 1087 (1970).
[10] A. R. H. Goodwin, M. D. Frorup, and E. H. Stenby, J. Chem. Thermodyn. **23**, 713 (1991).
[11] J. Adams Stratton, *Electromagnetic Theory* (McGraw-Hill, New York, 1941), pp. 545–554.
[12] N. Marcuwitz, *Waveguide Handbook* (McGraw-Hill, New York, 1951), Sec. 5.27.
[13] *A Physicist's Desk Reference*, edited by H. L. Anderson (AIP, New York, 1989), p. 128.
[14] A. F. Clark, G. E. Childs, and G. H. Wallace, in *Advances in Cryogenic Engineering*, edited by K. D. Timmerhaus (Plenum, New York, 1970), Vol. 15, pp. 85–90.
[15] L. A. Weber, Int. J. Thermophys. **13**, 1011 (1992).
[16] W. J. Rogers, F. Fontalba, E. F. Capps, J. C. Holste, K. N. Marsh, and K. R. Hall, Rev. Sci. Instrum. **59**, 193 (1988).
[17] H. Mansoorian, E. F. Capps, H. L. Gielen, P. T. Eubank, and K. R. Hall, Rev. Sci. Instrum. **46**, 1350 (1975).
[18] D. H. Ziger and C. A. Eckert, Rev. Sci. Instrum. **53**, 1296 (1982).
[19] H. B. Brugge, J. C. Holste, and K. R. Hall, Rev. Sci. Instrum. **63**, 5802 (1992).
[20] F. Weinhold, J. Chem. Phys. **86**, 1111 (1982).
[21] M. P. White and D. Gugan, Metrologia **29**, 37 (1992).
[22] T. K. Bose and R. H. Cole, J. Chem. Phys. **52**, 140 (1970).
[23] J. Gallagher, M. Huber, G. Morrison, and M. McLinden, *NIST Thermodynamic Properties of Refrigerants and Refrigerant Mixtures Database (REFPROP)*, NIST Standard Database 23 (National Institute of Standards and Technology, Gaithersburg, MD, 1992).
[24] A. R. H. Goodwin and G. Morrison, J. Phys. Chem. **96**, 5521 (1992).
[25] C. W. Meyer and G. Morrison, J. Chem. Eng. Data **36**, 409 (1991).
[26] C. W. Meyer and G. Morrison, J. Phys. Chem. **95**, 3860 (1991).
[27] J. C. Rainwater, in *Supercritical Fluid Technology: Reviews in Modern Theory and Applications*, edited by T. J. Bruno and J. F. Ely (Chemical Rubber, Boca Raton, FL, 1991), p. 57.
[28] G. X. Jin, S. Tang, and J. V. Sengers, Fluid Phase Equilibria **75**, 1 (1992).
[29] D. W. Burfield, H. P. Richardson, and R. A. Guereca, AIChE. J. **16**, 97 (1970).